Received Date : 02-Jul-2012

Revised Date : 22-Dec-2012

Accepted Date : 10-Jan-2013

Article type : Paper

Reference number: TER-2012-0056.R1
Received date: 02-Jul-2012
Revised version received date: 22-Dec-2012
Accepted date: 10-Jan-2013

Modeling the interseismic deformation of a thrust system: seismogenic potential of the Southern Alps

Salvatore Barba (a) (*)

Debora Finocchio (a) (b)

Elena Sikdar (c)

Pierfrancesco Burrato (a)

(a) Istituto Nazionale di Geofisica e Vulcanologia, Via di Vigna Murata 605, 00154 Roma, Italy

(b) Urbino University "Carlo Bo", Piazza della Repubblica 13, 61029 Urbino, Italy

(c) Birkbeck College, University of London, Malet Street, Bloomsbury, London, UK, WC1E 7HX. Now at Red Rock Resources Plc, London, UK.

This article has been accepted for publication and undergone full peer review but has not been through the copyediting, typesetting, pagination and proofreading process, which may lead to differences between this version and the Version of Record. Please cite this article as doi: 10.1111/ter.12026

(*) corresponding author: ph. No. +390651860362; email: salvatore.barba@ingv.it

Short title: Interseismic deformation of a thrust system.

Modeling the interseismic deformation of a thrust system: seismogenic potential of the Southern Alps

Salvatore Barba, Debora Finocchio, Elena Sikdar, and Pierfrancesco Burrato

Abstract

This paper focuses on the Montello Thrust System in the Eastern Southern Alps as a potential seismogenic source. This system is of particular interest because of its lack of historical seismicity. Nevertheless, the system is undergoing active deformation.

We developed a finite element model using visco-elasto-plastic rheology. The free parameters of the model, essentially, the locking status of the three thrusts included in the study, were constrained by matching the observed horizontal GPS and vertical leveling data.

We show that the amount of interseismic fault locking, and thus the seismic potential, is not necessarily associated with the fastest-slipping faults. More specifically, the locked Bassano thrust has a greater seismic potential than the freely slipping Montello thrust. Our findings suggest that

faults with subtle evidence of Quaternary activity should be more carefully considered when creating seismic hazard maps.

Keywords: seismogenic potential, thrust fault, rheology, Alps, earthquakes

Introduction

Numerous geological and geodetic observations and models have been made to constrain interseismic crustal deformation in response to the locking of thrust faults (e.g., Simoes *et al.*, 2004; Moreno *et al.*, 2010). It is generally not difficult to fit most of the data by adjusting model parameters. The challenge is to establish from the data a first-order deformation pattern that allows the exploration of possible seismogenic processes (Wang, 2007).

Locked faults are potentially seismogenic (Chlieh *et al.*, 2004; Moreno *et al.*, 2010). Conversely, in the presence of unlocked faults, the strain is gradually released and is sometimes observed at the surface using geodetic methods (Dragert *et al.*, 2001). Two-dimensional finite element models accounting for mechanical layering, faults, and creep rheologies are able to fit the available constraints on interseismic and long-term surface displacements (e.g., Vergne *et al.*, 2001; Hsu *et al.*, 2003; Chamlagain and Hayashi, 2005).

In this study, the Montello Thrust System (MTS) of the Eastern Southern Alps (Fig. 1) in Northern Italy was used as a regional example for determining the interseismic behavior and seismogenic potential of locked faults. Due to the fault size (larger than 200 km^2, which may result in earthquakes with magnitudes of up to M6.5), the unclear link with major historical earthquakes, and the urban and industrial drift of the area, the MTS is considered to pose a large seismic risk in the area (Slejko *et al.*, 2008). We modeled the interseismic deformation of the MTS occurring in an elasto-visco-plastic medium using the available geodetic data as a constraint.

Geological setting

The Eastern Southern Alps, located in the northern part of the continental Adriatic plate, are a Neogene south-verging thrust belt representing a retro-belt in the Alpine edifice. The upper crust (Qd and Cf in Fig. 2) consists of a sedimentary cover (mainly Permo-Triassic carbonate-built rocks, Paleogenic flysch, and Quaternary deposits). The intermediate crust consists of a metamorphosed crystalline basement, which in the Southern Alps is mostly composed of quartz-built rocks intruded by granitic bodies, overlying the Adriatic crust (Castellarin *et al.*, 2006).

The 160-km-long sector from the Schio-Vicenza line to the Dinaric Range undulates by 10-12 km along Mesozoic-inherited features and has accommodated a minimum shortening of 30 km since the Neogene (see, e.g., Zanferrari *et al.*, 1982; Doglioni, 1992), ~20 km of which lies across a ~30-km-long section (Castellarin *et al.*, 2006).

The MTS consists of three faults (Fig. 2): the Bassano and Montello thrusts and the Montello back-thrust, an antithetic fault that originated at the top of the basement. The basal detachment of the thrust belt is located within the basement at a depth of 12-15 km (Castellarin *et al.*, 2006; Doglioni and Carminati, 2008).

On the southern limb of the Bassano anticline, clastic sedimentation exhibits onlap geometries and reduced thicknesses (Doglioni, 1992). This “triangle zone” indicates the presence of a growth fold from the Late Oligocene to the Quaternary and suggests the necessity of a thrust to resolve the volume problem in the Bassano structural high. The Montello anticline has been undergoing high uplift rates since the Holocene (Benedetti *et al.*, 2000), suggesting that the Montello thrust is blind and active.

Rheology of the area

The ongoing collision processes (shortening rate of ~2 mm/y; Ward, 1994; Caporali *et al.*, 2011) make the Alps a seismically active belt (e.g., Slejko *et al.*, 1989; Cuffaro *et al.*, 2010). For instance, the largest known earthquakes (Rovida *et al.*, 2011) have been located around the Brenta River (year 1695, M6.5), at the eastern termination of the Bassano thrust (year 1873, M6.3), and around the Tagliamento River (year 1976, M6.5; the magnitudes represent cumulative macroseismic effects). Across the MTS, however, few and small-magnitude historical earthquakes point to a minimum in the seismic moment release.

Here, the microseismicity recorded during a local experiment is located mainly in the basement, down to depths of 15 km (Fig. 2; Chiaraluce *et al.*, 2009), with positive P-wave velocity anomalies and Vp/Vs ratios (Anselmi *et al.*, 2011). Below a depth of 15 km, seismic bulletins report few instrumental earthquakes (ISIDe Working Group, 2010). A geothermal gradient of 22±3 °C/km (Viganò *et al.*, 2012) results in a temperature of 330±45 °C at a depth of 15 km, a temperature that is generally compatible with the observed variations in the depth cut-off of seismicity (Bird and Kong, 2004). Thus, the so-called “brittle-ductile” transition is possibly located at a depth of 15 km.

Given the temperature gradient, most of the crystalline basement at depths greater than 15 km would flow by dislocation creep (viscous non-Newtonian rheology; Viganò *et al.*, 2012), compatible with the earthquake-depth distribution. Moreover, the upper crust, because it is mostly composed of carbonates, may accommodate some strain by diffusive mass transfer processes, such as pressure solution and precipitation. The latter process is typically a viscous-type deformation mechanism with a Newtonian rheology and strong dependence on grain size.

Given the viscous behavior of the lower crust and the contribution of the diffusive mass transfer in the upper crust of the Southern Alps, we performed interseismic modeling assuming an elasto-plastic-viscous rheology.

Data

Horizontal GPS velocities and terrestrial leveling data were used to validate the numerical model. We focused on the sector of the Po Plain and the Venetian Prealps, where the thrust front deviates approximately 10-12 km from cylindricity for 160 km between the Schio-Vicenza tectonic line and the Dinaric range (Fig. 1). In this sector, the horizontal GPS velocities from Caporali *et al.* (2011) were projected along the section A-A’ (Fig. 3). The section-parallel component was filtered by convolution with a Gaussian function with widths of 100 and 50 km (Fig. 4a). This low-pass filter was used to remove outliers or high-frequency noise from the data.

Terrestrial leveling was performed by the Istituto Geografico Militare during surveys between 1949 and 1977 (IGM-RG, 1978; Teatini *et al.*, 2005) over a distance of ~200 km over steep topography, from the Po plain to the Alps mountain belt (Fig. 4b,c). A terrain-correlated bias of 0.027 °/yr was removed, and the confidence interval was computed.

Hereinafter, ‘Vh’ indicates the filtered section-parallel component of the horizontal GPS velocities, and ‘Vv’ indicates the range of the confidence interval of the corrected leveling data. Thus, Vh and Vv represent the horizontal and vertical relative velocities, respectively, along the section of Fig. 2.

Numerical model

Based on the geological section considered in this study (Fig. 2), we developed a model and finite-element mesh (Fig. 5). The simulations were performed using Marc release 2010 (MSC.Software, 2010) with four-node elements using a plane-strain approximation. The 2D mesh (60 km long and 40 km deep) was composed of 2582 elements (~1 km^2) and 2714 nodes. Because we modeled only surface data, the faults were incorporated as zero-friction (free-slip) discontinuities. The upper layer (carbonates) was an elastic-plastic medium, the intermediate layer (basement) was elastic, and the lower layer was a viscoplastic medium. The upper and lower layers had a yield stress ▯ of 100 MPa. All strata had a density of 2300 kg/m^3, a Young’s modulus E of 9 GPa, and a Poisson's ratio ▯ of 0.3. The model was subject to the force of gravity and was pre-stressed.

Along the southern edge of the model (located in the Veneto plain), the nodes from depths of 0 to 15 km were locked in the horizontal direction. From 15 to 40 km, we applied 8 m of northward displacement. Along the northern edge (located in the Alps foothills), we applied 7 m of southward displacement from depths of 0 to 21 km and horizontal locking from 21 to 40 km (Fig. 5). The northward displacement applied to the lower layer represents the underthrusting of the Adriatic lithosphere. The southward displacement applied to the upper and intermediate layers represents the effect of the Alps belt on the upper crust. The bottom of the model was locked in the vertical direction. The model was run for 8000 years.

The parameters tested include the ▯, E, ▯, width and length of the model, and presence or absence of faults (Table 1). The fault dip was varied from 30 to 50°. The position and length of the unlocked (free-slip) segment along the faults were tested from 0 to 36 km. We combined a number of parameter combinations. Table 1 shows the range of all of the parameters tested along with a synthetic description of the results, which will be discussed later. The rheological parameters were used for the upper and lower layers independently, i.e., one quantity was perturbed, whereas the other two were set at the best-fit values (Table 1).

We simulated ~160 models and selected the models that best fit, based on the least-squares error, the filtered data.

Modeling results

Hereinafter, long- and short-wavelength models indicate the models that fit the V_h filtered at 100 and 50 km, respectively. The free parameters of the model were fundamentally the locking statuses of the three thrusts included in the MTS.

In the long-wavelength model, the horizontal velocity decreases northward from 1 to 0.2 mm/yr, with a rate change at 30 km (Fig. 6a). The model fits the V_h reasonably well, although the data, unlike the model, exhibit a continuous decrease in velocity.

'

A nearly perfect fit is derived from the short-wavelength model: the horizontal velocity decreases between 0 and 15 km and between 30 and 50 km, matching the V_h data very well (Fig. 6b). The vertical velocity increases by ~1 mm/yr in the northward direction (Fig. 6d). In the first half of the section, the model velocity fits the Vv well; however, in the second half, there is a mismatch. The short-wavelength model is compatible with the available data (Fig. 6b,d) and thus represents the best model. This model is characterized by free-slip along the part of the Bassano thrust (6 km) embedded in the lower layer and along the Montello thrust (33 km) and back-thrust (5 km; Fig. 7).Varying the dip of the fault by ±10° does not significantly affect the results. The remaining portions of the faults are locked. The best-fit parameters are listed in Table 1.

The surface velocity mainly depends on the presence of the wide unlocked portion of the Montello thrust and on the rheological stratification; the unlocked portions of the back-thrust and Bassano thrust play a minor role.

To study the effect of the stratification in the best model, considered as the reference, we perturbed the values of E (from 1 to 50 GPa), ⍰ (from 1 MPa to 1 GPa), and ⍰ (from 0.2 to 0.4). Varying ⍰ and ⍰ induced negligible effects. E was the most significant parameter and produced the largest changes in the simulated velocities. Augmenting E in the elastic intermediate layer caused the horizontal velocity to diminish with respect to the reference model and the vertical velocity to increase between 0 and 40 km and decrease between 40 and 60 km (Fig. 8a). Augmenting E in the upper layer is equivalent to reducing E in the intermediate layer. On the other hand, decreasing E in the upper layer allows the horizontal velocity to increase between 0 and 40 km and the vertical velocity to decrease between 30 and 60 km.

Discussion and conclusions

Being calibrated with short-term data and with no earthquakes in the observation period, our best model well represents the interseismic behavior of the MTS. The boundary conditions, modeled faults, and rheological parameters will be the framework in which the rate of loading and the seismic potential of additional, and possibly locked, faults can be computed. The best model, i.e., the model that best simulates the data, predicts the locked status of the fault segments (Fig. 7).

Our model, which adopted a simplified stratigraphy and a 2D realization, was sufficient to reproduce the gross characteristics of the surface velocity. Minor faults, which are present in reality, are absent in the modelled cross-section. However, we did not try recovering details from the data but only the general fault behavior (locked vs. unlocked); investigating the fault dip or geometry requires a more refined analysis and a denser dataset.

The model simulated the observed vertical velocity rather well given the various constraints (Fig. 6). In the Montello anticline, our modeled uplift rate (0.5 mm/y) is comparable to the 0.49-0.87 mm/y rate identified by Benedetti *et al.* (2000), who correlated the ages of fluvial terraces predicted by assuming a constant uplift rate with the ages of marine high-stands, and with the 0.32-0.4 mm/y minimum uplift rate constrained by the depth of the Quaternary deposits in the footwall of the fault (Galadini *et al.*, 2005). Our solution minimizes the difference using the horizontal velocities, which are favored because GPS data are subject to more verification procedures; however, this approach represents a compromise in reproducing the vertical velocities.

Microseismicity occurs diffusely in the basement (Fig. 2) and clusters around the 2-MPa stress patch induced by the Montello thrust (see Fig. AF3 in the supplementary material). No microseismicity appears to have occurred near the Bassano thrust, which is compatible with its predicted locked state.

The Montello thrust and back-thrust may be creeping (Fig. 7). At shallow depths, velocity-strengthening gouges dominate (Scholz, 2002). At greater depths, stress-driven creep may occur through nearly aseismic slip or creep events when the tectonic stress plus the local stress concentration exceeds the fault strength or the (constant or, equivalently, zero) resistive shear stress (e.g., Li and Rice, 1987; Savage and Lisowski, 1993). The Bassano thrust is locked in the depth range where velocity-weakening behavior is expected (Marone and Scholz, 1988), which suggests the potential for the induction of large earthquakes. Whilst the Montello thrust is parameterized as a seismogenic fault (Mw=6.5) for seismic hazard mapping in Italy, the Bassano thrust is not (DISS Working Group, 2010). Thus, future studies of the Bassano thrust are urgently needed to disprove its hazard or existence or to quantify its present-day slip rate and seismogenic potential.

Based on the modeling of the first-order deformation pattern, we conclude that, unlike the freely slipping Montello thrust, the Bassano thrust may bear a large seismogenic potential, because it is locked in interseismic time. Performing interseismic modeling on more refined data can effectively facilitate future research by identifying locked, potentially seismogenic faults in a thrust system.

Acknowledgements

We thank the editor Carlo Doglioni and three anonymous referees for their thorough reviews and comments, which improved the manuscript. We thank Roberto Basili and Michele Carafa for discussions and Paolo Marco De Martini for discussions and for providing the IGM terrestrial leveling data used in this study. ES performed the sensitivity tests during her internship at INGV.

References

Anselmi, M., Govoni, A., De Gori, P., Chiarabba, C., 2011. Seismicity and velocity structures along the south-Alpine thrust front of the Venetian Alps (NE-Italy). Tectonophysics, **513**, 37-48. doi:10.1016/j.tecto.2011.09.023

Benedetti, L. P., Tapponnier, G., King, C. P., Meyer B., Manighetti, I. 2000. Growth folding and active thrusting in the Montello region, Veneto, northern Italy. J. Geophys. Res., **105(B1)**, 739-766.

Burrato, P., Poli, M. E., Vannoli, P., Zanferrari, A., Basili, R., Galadini, F., 2008. Sources of Mw 5+ earthquakes in northeastern Italy and western Slovenia: an updated view based on geological and seismological evidence. Tectonophysics, **453**, 157-176, doi:10.1016/j.tecto.2007.07.009.

Bird, P., Kong, X., 1994. Computer simulations of California tectonics confirm very low strength of major faults. Geol. Soc. Am. Bull., **106** (2), 159-174.

Caporali, A., Barba, S., Carafa, M.M.C., Devoti, R., Pietrantonio, G., Riguzzi, F., 2011. Static stress drop as determined from geodetic strain rates and statistical seismicity. J. Geophys. Res., **116**, B02410, doi:10.1029/2010JB007671.

Castellarin A., Nicolich R., Fantoni R., Cantelli L., Sella M. & Selli L. 2006. Structure of the lithosphere beneath the Eastern Alps (southern sector of the TRANSALP transect). Tectonophysics, **414**, 259-282.

Castellarin, A., Vai, G. B., Cantelli, L., 2006. The Alpine evolution of the Southern Alps around the Giudicarie faults: A Late Cretaceous to Early Eocene transfer zone. Tectonophysics, **414**, 203-223, doi:10.1016/j.tecto.2005.10.019.

Chamlagain, D. and Hayashi, D., 2005. Neotectonic fault analysis by 2D finite element modeling for studying the Himalayan fold-and-thrust belt in Nepal. J. Asian Earth Sci., **29**, 473-489. doi:10.1016/j.jseaes.2005.10.016.

Chiaraluce, L., Valoroso, L., Anselmi, M., Bagh, S., Chiarabba, C., 2009. A decade of passive seismic monitoring experiments with local networks in four Italian regions. Tectonophysics, **476**, 85-98. doi:10.1016/j.tecto.2009.02.013

Chlieh, M., De Chabalier, J. B., Ruegg, J. C., Armijo, R., Dmowska, R., Campos, J., Feigl, K. L., 2004. Crustal deformation and fault slip during the seismic cycle in the North Chile subduction zone, from GPS and InSAR observations. Geophys. J. Int., **158**, 695-711. doi:10.1111/j.1365-246X.2004.02326.x

Cuffaro, M., Riguzzi, F., Scrocca, D., Antonioli, F., Carminati, E., Livani, M., Doglioni, C., 2010. On the geodynamics of the northern Adriatic plate. Rend. Fis. Acc. Lincei, **21** (Suppl 1), S253-S279, DOI 10.1007/s12210-010-0098-9.

Devoti, R., Riguzzi, F., Cuffaro, M., Doglioni C., 2008. New GPS constraints on the kinematics of the Apennines subduction. Earth Planet. Sci. Lett., **273**, 163-174.

DISS Working Group, (2010). Database of Individual Seismogenic Sources (DISS), Version 3.1.1: A compilation of potential sources for earthquakes larger than M 5.5 in Italy and surrounding areas. http://diss.rm.ingv.it/diss/, © INGV 2010 - Istituto Nazionale di Geofisica e Vulcanologia - All rights reserved. Last accessed date: December 18, 2012.

Doglioni, C., 1992. The Venetian Alps thrust belt. In: K.R. McClay (Ed): Thrust Tectonics, Chapman & Hall, 319-324, London.

Doglioni, C., 1992. Relationships between Mesozoic extensional tectonics, stratigraphy and Alpine inversion in the Southern Alps. Eclogae Geologicae Helvetiae, **85**, 1, 105-126.

Doglioni, C., 1992. Main differences between thrust belts. Terra Nova, 4, 2, 152-164.

Doglioni, C., Barba, S., Carminati, E., & Riguzzi, F., 2011. Role of the brittle-ductile transition on fault activation. *Phys. Earth Planet. Int.*, **184**, 160–171.

Doglioni, C., Carminati, E., 2008. Structural styles and Dolomites field trip. Mem. Descr. Carta Geol. It., **82**, 1-299.

Dragert, H., Wang, K., James, T. S., 2001. A Silent Slip Event on the Deeper Cascadia Subduction Interface. Science, 292 (5521), 1525-1528 DOI:10.1126/science.1060152.

Fantoni, R., Barbieri, C., Catellani, D., Castellarin, D., Di Giulio, A., & Pessina, C., 2001. The record of south-Alpine events in the Venetian foreland and foredeep. Geol. Paloaont. Mitt. Innsbruck, **25**, 79–81.

Galadini, F., Poli, M.E., Zanferrari, A., 2005. Seismogenic sources potentially responsible for earthquakes with M≥6 in the eastern Southern Alps (Thiene–Udine sector, NE Italy). Geophys. J. Int., **161**, 739-762. doi: 10.1111/j.1365-246X.2005.02571.x

Hsu, Y.-J., Simons, M., Yu, S.-B., Kuo, L.-C., Chen, H.-Y., 2003. A two-dimensional dislocation model for interseismic deformation of the Taiwan mountain belt. Earth Planet. Sci. Lett., **211**, 287-294. doi: 10.1016/S0012-821X(03)00203-6.

IGM-RG, 1978. Relazione sui lavori di triangolazione eseguiti nel Friuli dall’Istituto Geografico Militare nell’anno 1977. Reparto Geodetico, Firenze.

ISIDe Working Group (INGV, 2010), Italian Seismological Instrumental and parametric database: http://iside.rm.ingv.it/. Last accessed date: December 18, 2012.

Konca, A.O., Avouac, J., Sladen, A., Meltzner, A. J., Sieh, K., Fang, P., Li, Z., Galetzka, J., Genrich, J., Chlieh, M., Natawidjaja, D. H., Bock, Y., Fielding, E.J., Ji, C., Helmberger, D.V., 2008. Partial rupture of a locked patch of the Sumatra megathrust during the 2007 earthquake sequence. Nature, **456**, 631-635. doi:10.1038/nature07572.

Li, V. C. and J. R. Rice (1987), Crustal deformation in Great California earthquake cycles, *J. Geophys. Res.*, **92**(B11), 11,533–11,551, doi:10.1029/JB092iB11p11533.

Marone, C., and C. H. Scholz (1988), The depth of seismic faulting and the upper transition from stable to unstable slip regimes, Geophys. Res. Lett., **15**, 621–624, doi:10.1029/GL015i006p00621.

Meltzner, A., Sieh, K., Abrams, M., Agnew, D., Hudnut, K., Avouac, J. and Natawidjaja, D. 2006. Uplift and subsidence associated with the great Aceh-Andaman earthquake of 2004. J. Geophys. Res. 111(B2): doi: 10.1029/2005JB003891.

Moreno, M., Rosenau, M., Oncken, O., 2010. 2010 Maule earthquake slip correlates with pre-seismic locking of Andean subduction zone. Nature, **467**, 198-202. doi:10.1038/nature09349

MSC.Software Corporation, Home Page (2010). MSC.Software Corporation - <http://www.mscsoftware.com/>. Last accessed date: December 18, 2012.

Rovida, A., Camassi, R., Gasperini, P., Stucchi, M. (eds.), 2011. CPTI11, the 2011 version of the Parametric Catalogue of Italian Earthquakes. Milano, Bologna, <http://emidius.mi.ingv.it/CPTI/>, Last accessed date: December 18, 2012.

Savage, J. C. and M. Lisowski (1993), Inferred depth of creep on the Hayward Fault, central California, *J. Geophys. Res.*, **98**(B1), 787–793, doi:10.1029/92JB01871.

Scholz, C., 2002. The mechanics of Earthquakes and Faulting, Cambridge University Press.

Simoes M., J.P. Avouac, R. Cattin, and Henry, P. (2004). The Sumatra subduction zone: A case for a locked fault zone extending into the mantle. J. Geophys. Res., 109, B10402, doi:10.1029/2003JB002958.

Slejko, D., Carulli, G.B., Carraro, F., Castaldini, D., Cavallin, A., Doglioni, C., Iliceto, V., Nicolich, R., Rebez, A., Semenza, E., Zanferrari, A., Zanolla, C., 1987. Modello sismotettonico dell'Italia Nord-Orientale. C.N.R. G.N.D.T. Rendiconto n. 1, Ricci, Trieste, 83 pp.

Slejko, D., G. B. Carulli, R. Nicolich, A. Rebez, A. Zanferrari, A. Cavallin, C. Doglioni, F. Carraro, D. Castaldini, V. Iliceto, E. Semenza and C. Zanolla, 1989. Seismotectonics of the eastern Southern-Alps: a review. Boll. Geof. Teor. Appl., 31, 109-136.

Slejko, D., Rebez, A., Santulin, M., 2008. Seismic hazard estimates for the Vittorio Veneto broader area (N.E. Italy). Boll. Geofis. Teor. Appl., **49**, 329–356.

Teatini, P., Tosi, L., Strozzi, T., Carbognin, L., Wegmüller, U., Rizzetto, F., 2005. Mapping regional land displacements in the Venice coastland by an integrated monitoring system. Remote Sensing of Environment, 98 (4), 403-413, doi:10.1016/j.rse.2005.08.002.

Ward, S. N., 1994. Constraints of the seismotectonics of the central Mediterranean from Very Long Baseline Interferometry. Geophys. J. Int., **117**, 441-452.

Wyss, M., Nekrasova, A. & Kossobokov, V. (2012) - Errors in Expected Human Losses Due to Incorrect Seismic Hazard Estimates. In press on Natural Hazards.

Vergne, J., Cattin, V., Avouac, J. P., 2001. On the use of dislocations to model interseismic strain and stress build-up at intracontinental thrust faults. Geophys. J. Int., **147**, 155-162.

Viganò A., Della Vedova B., Ranalli G., Martin S, and Scafidi D., 2012. Geothermal and rheological regime in the Po plain sector of Adria (Northern Italy), *Italian Journal of Geosciences*, **131**(2), 228-240, doi: 10.3301/IJG.2012.09.

Wang, K., 2007. Elastic and viscoelastic models of crustal deformation in subduction earthquake cycles. In *The Seismogenic Zone Of Subduction Thrust Faults*, edited by T. Dixon and J. C. Moore, Columbia University Press, New York, NY, 680 p.

Zanferrari A., Bollettinari G., Carobene L., Carton A., Carulli G. B., Castaldini D., Cavallin A., Panizza M., Pellegrini G. B., Pianetti F., Sauro U., 1982. Evoluzione neotettonica dell' Italia Nord Orientale. *Mem. Soc. Geol.*, **35**, 355-376.

Figure Captions

Figure 1. Thrust and strike-slip fault systems of the Eastern Southern Alps and western Slovenia (modified from Burrato *et al.*, 2008). The faults discussed in the text are highlighted in bold. Composite (gray bands) and Individual Seismogenic Sources (rectangles) from the DISS database are also shown (DISS Working Group, 2010). The trace of the geodetic line is indicated by the dashed line. The background is represented by the SRTM DEM (Void-filled seamless SRTM data V1, 2004, International Centre for Tropical Agriculture (CIAT), available from the CGIAR-CSI SRTM 90 m Database: http://srtm.csi.cgiar.org). Legend: MT: Montello thrust; MB: Montello back-thrust; BT: Bassano thrust.

Figure 2. Simplified geological section across the Montello thrust system (see Fig. 1 for section trace; modified from Doglioni, 1992; Galadini *et al.*, 2005; Castellarin *et al.*, 2006). Dip values are approximated. Bas: metamorphosed crystalline basement, mostly composed of quartz-built rocks, intruded by granitic bodies; Cf: Permo-Triassic carbonate rocks and Paleogenic flysch; Qd: Oligo-Miocene Molasse succession and Quaternary deposits (see Fantoni *et al.*, 2001, for details). Gray dots and black star: earthquakes (from Chiaraluce *et al.*, 2009).

Figure 3. Schematic map showing the trace of the numerical model (A-A') and the trace of the geological section (a; dashed gray line). Arrows represent GPS data with error ellipses of 1σ (from Caporali *et al.*, 2011); triangles indicate the GPS stations used in this work. The solid gray line represents the trace of the leveling data. MT: Montello thrust, BT: Bassano thrust.

Figure 4. Data. (a) Horizontal velocity Vh, (b) topography, and (c) uncorrected vertical velocity Vv* with confidence intervals. Data are projected onto the model section A-A'.

Figure 5. Geometry, mesh, and boundary conditions of the numerical model. The arrows along the edges represent the applied displacement; the circles indicate zero orthogonal displacement. MT:

Montello thrust; BT: Bassano thrust; MB: Montello back-thrust; UL: upper layer; IL: intermediate layer; LL: lower layer.

Figure 6. Best-fit models for 50-km (short-) and 100-km (long-wavelength) widths. (a, b) horizontal and (c, d) vertical surface velocities for (a, c) long-wavelength and (b, d) short-wavelength models. Continuous lines: filtered data; gray bands: range of confidence intervals; dashed lines: model. The RMS is used to compare the performances of the different models (see supplementary material, section S2, for details).

Figure 7. Diagram of the model results showing locked and unlocked portions of the Montello thrust (MT), Montello back-thrust (MB), and Bassano thrust (BT). The vertical scale is cut at utile depth.

Figure 8. Sensitivity tests for the Young's modulus E (a: model vertical velocity Vv; b: model horizontal velocity Vh). We tested the upper and intermediate layers separately. The reference is the short-wavelength model (see Fig. 6b,d).

Table 1. Tested parameters, model results, and best-fit values.

Parameter	Long-wavelength model	Range	Values or step	Effect of UL	Effect of IL	Short-wavelength model – best-fit values
Yield Stress ⍰	100 MPa	1-1000 MPa	1, 10, 50, 100, 500, 1000 MPa	Vh: + Vv: +	(*)	100 MPa
Young's Modulus E	9 GPa	0.1-50 GPa	0.1, 1, 9, 10, 50 GPa	Vh: - Vv: (*)	Vh: - Vv: (*)	9 GPa

Poisson's Ratio ⍰	0.3	0.2-0.4	0.2, 0.3, 0.4	Vh: - Vv: +	Vh: + Vv: +	0.3
Length	60 km	50-150 km	Step 10 km	(*)	(*)	60 km
Width (Total)	40 km	30-50 km	Step 5 km	(*)	(*)	40 km
Width (UL; left edge)	8 km	5-15 km	Step 1 km	(*)	(*)	8 km
Width (UL; right edge)	11 km	7-21 km	Step 1 km	(*)	(*)	11 km
Presence of faults	MT	83 combinations	MT, MB, BT, LAD	(*)	(*)	MT, MB and BT
Fault dip	MT: 45°	MT: 30-50° MB: 30-50° BT: 30-40°	Step 5°	(*)	(*)	MT: 45° MB: 50° BT: 30°
Fault width	MT:18 km	MT: 0-36 km MB: 0-9 km BT: 0-20 km LAD: 0-10 km	Step 1 km	(*)	(*)	MT: 33 km MB: 5 km BT: 6 km LAD: 0 km

UL: upper layer; IL: intermediate layer; MT: Montello thrust; MB: Montello back-thrust; BT: Bassano thrust; LAD: low-angle discontinuity (top of the basement); Vh: effect on horizontal velocity; Vv: effect on vertical velocity; + = positive correlation; - = negative correlation; (*) not significant and/or not shown.

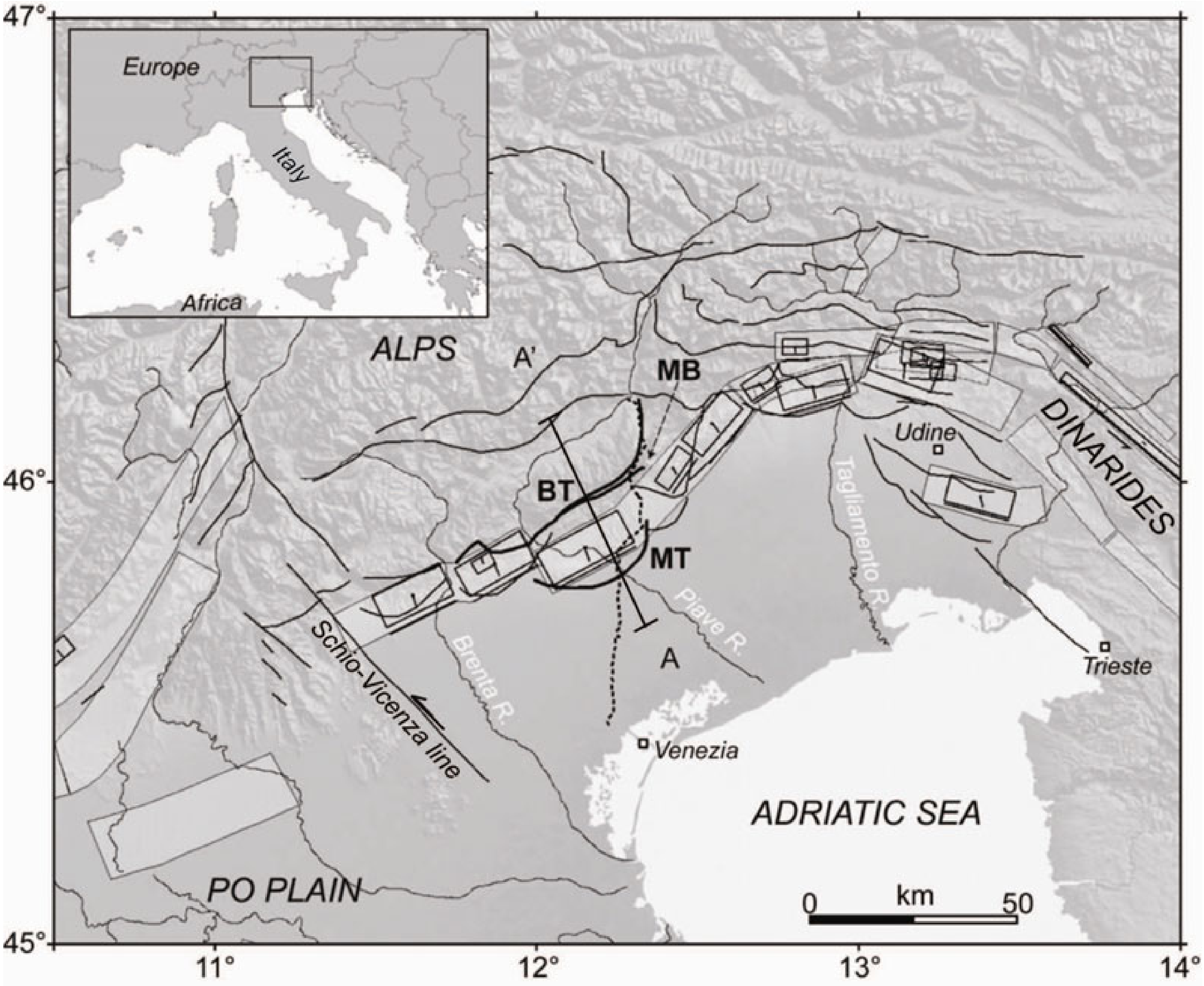
47°
46°
45°
11°
12°
13°
14°
Europe
Italy
Africa
ALPS
A'
MB
BT
MT
A
Udine
DINARIDES
Tagliamento R.
Piave R.
Brenta R.
Schio-Vicenza line
Venezia
Trieste
ADRIATIC SEA
PO PLAIN
0
km
50

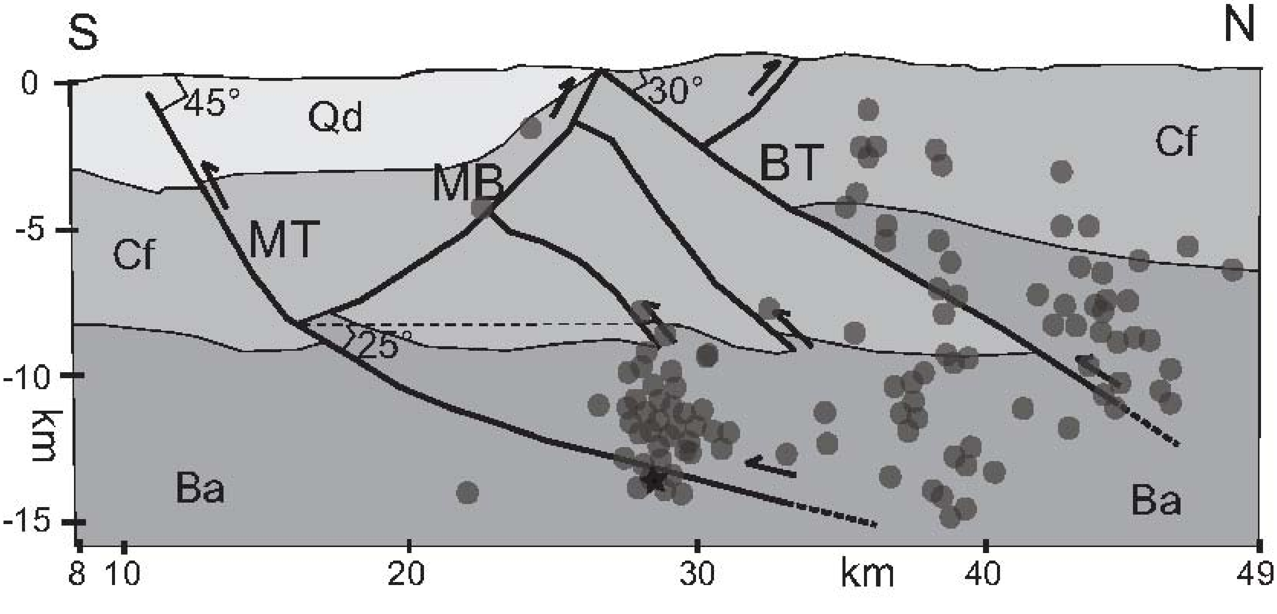
S
N
0
-5
-10
-15
km
45°
30°
25°
Qd
Cf
MB
MT
BT
Cf
Ba
Ba
8
10
20
30
km
40
49

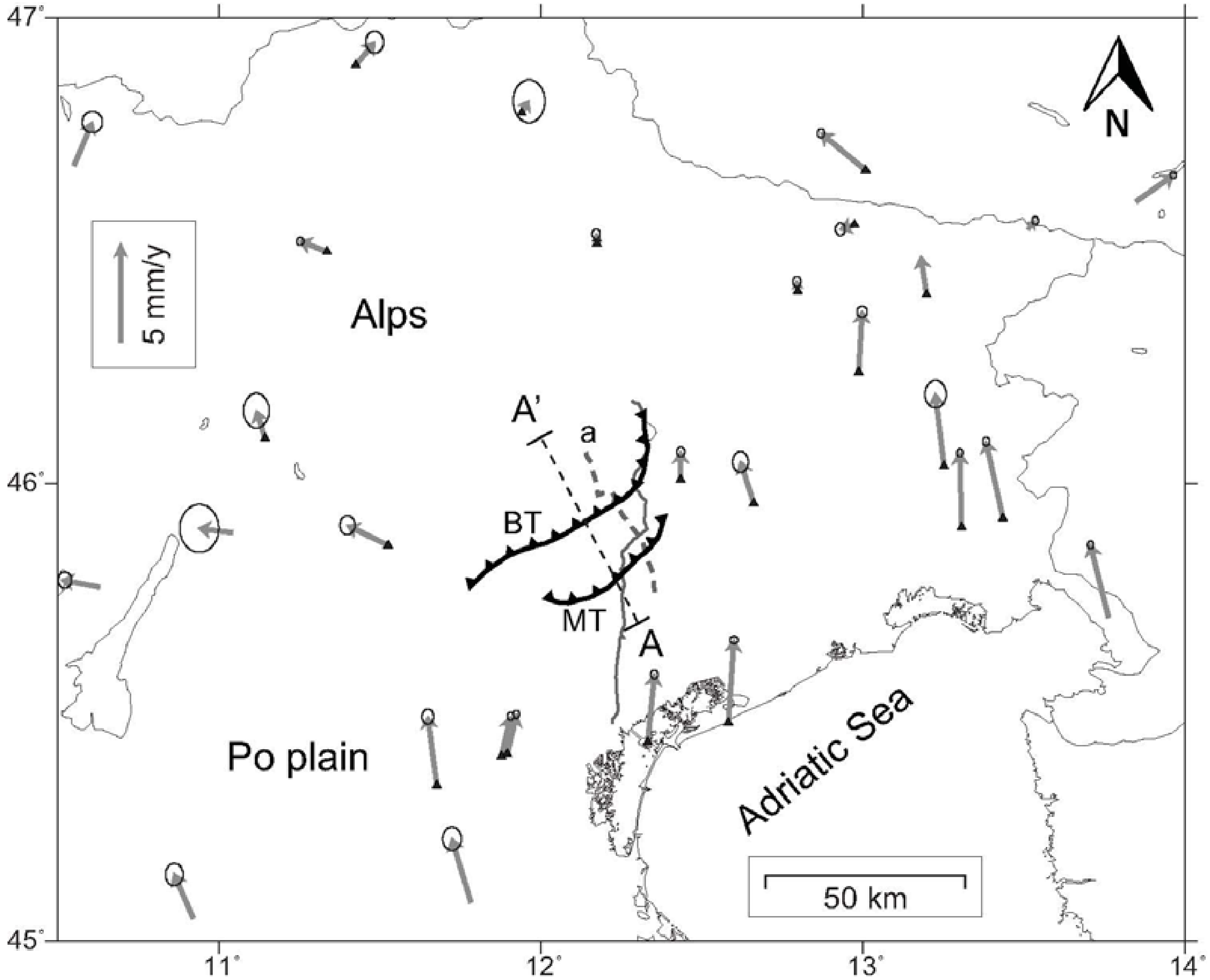
47°
46°
45°
11°
12°
13°
14°
N
5 mm/y
Alps
A'
a
BT
MT
A
Po plain
Adriatic Sea
50 km

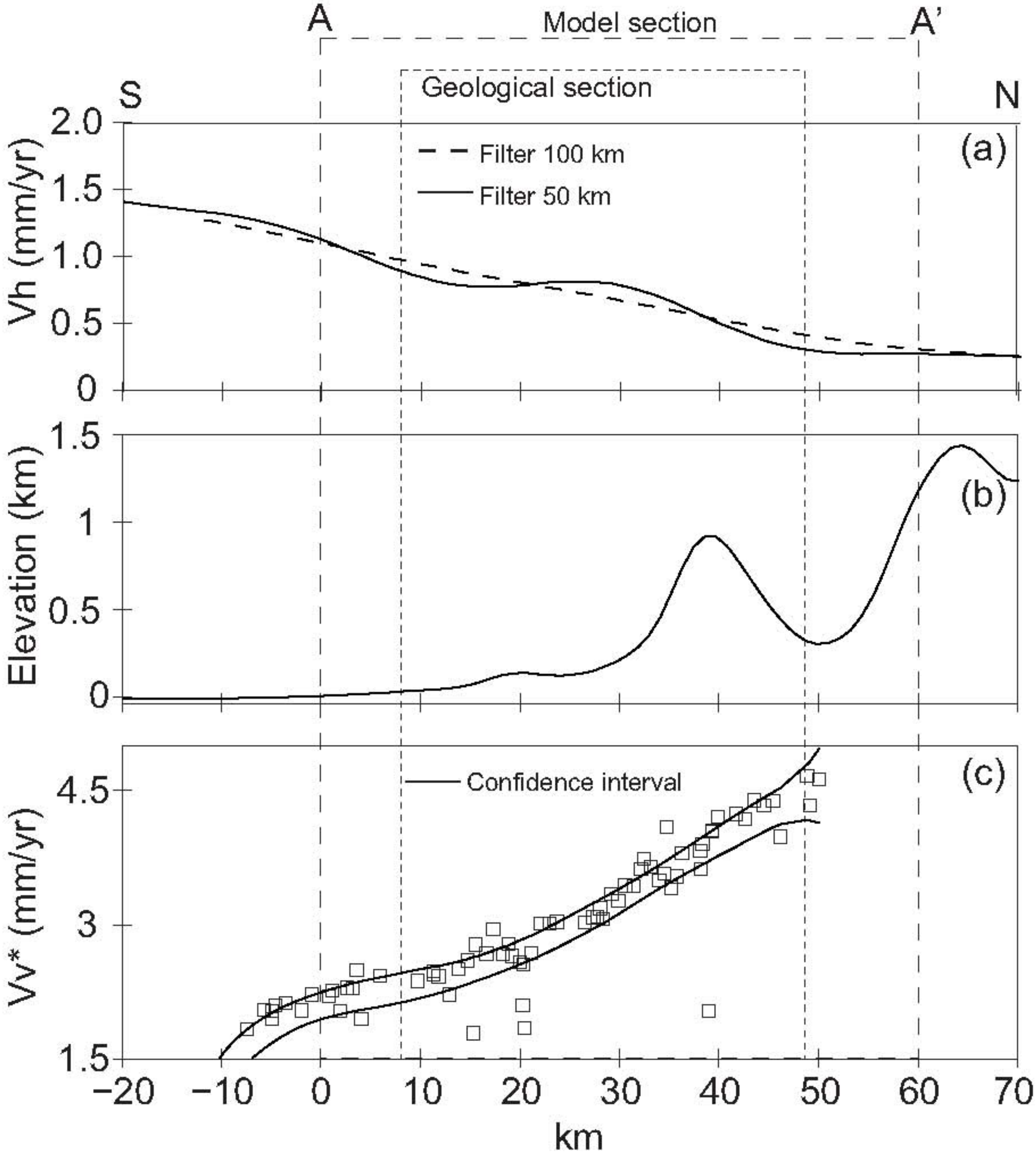
A
Model section
A'
Geological section
S
N
2.0
1.5
1.0
0.5
0
Vh (mm/yr)
(a)
Filter 100 km
Filter 50 km
1.5
1
0.5
0
Elevation (km)
(b)
4.5
3
1.5
Vv* (mm/yr)
(c)
Confidence interval
−20
−10
0
10
20
30
40
50
60
70
km

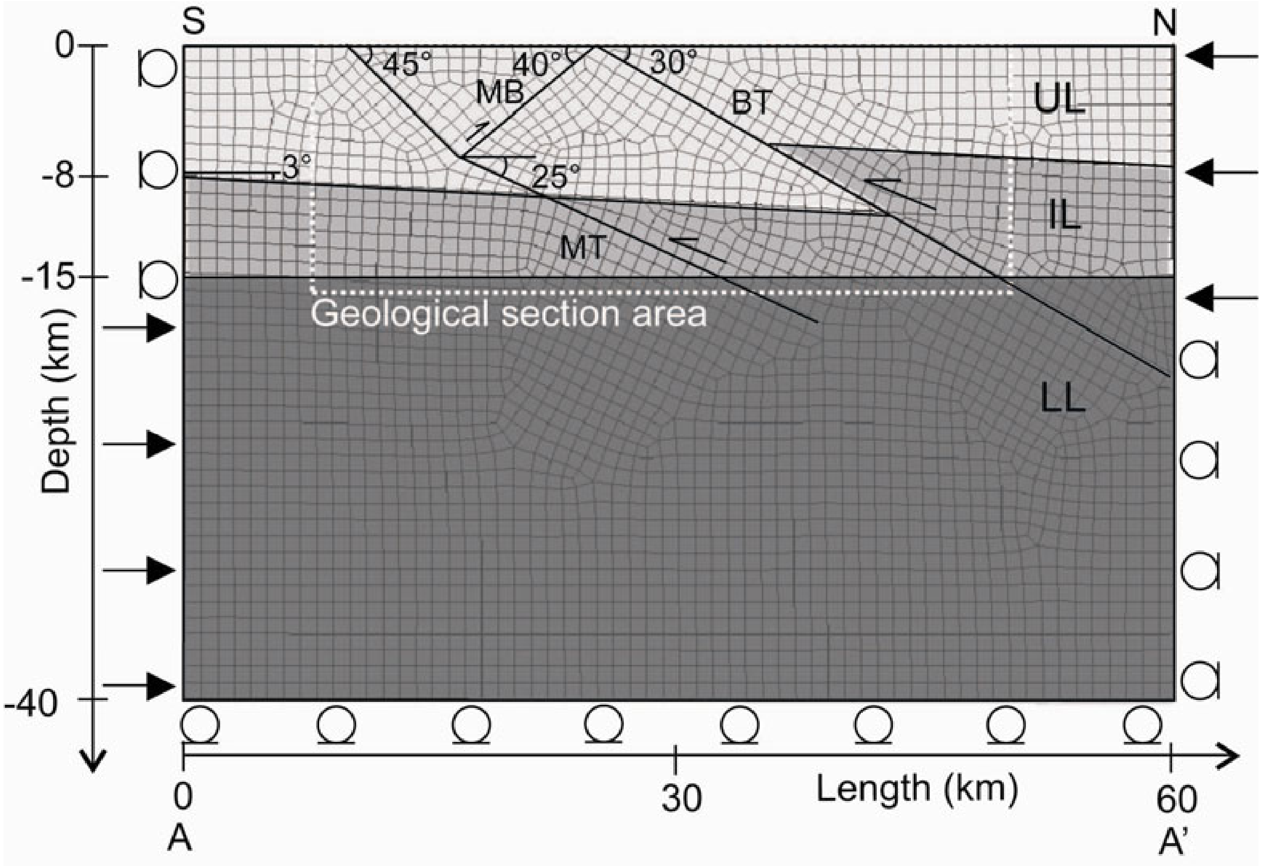

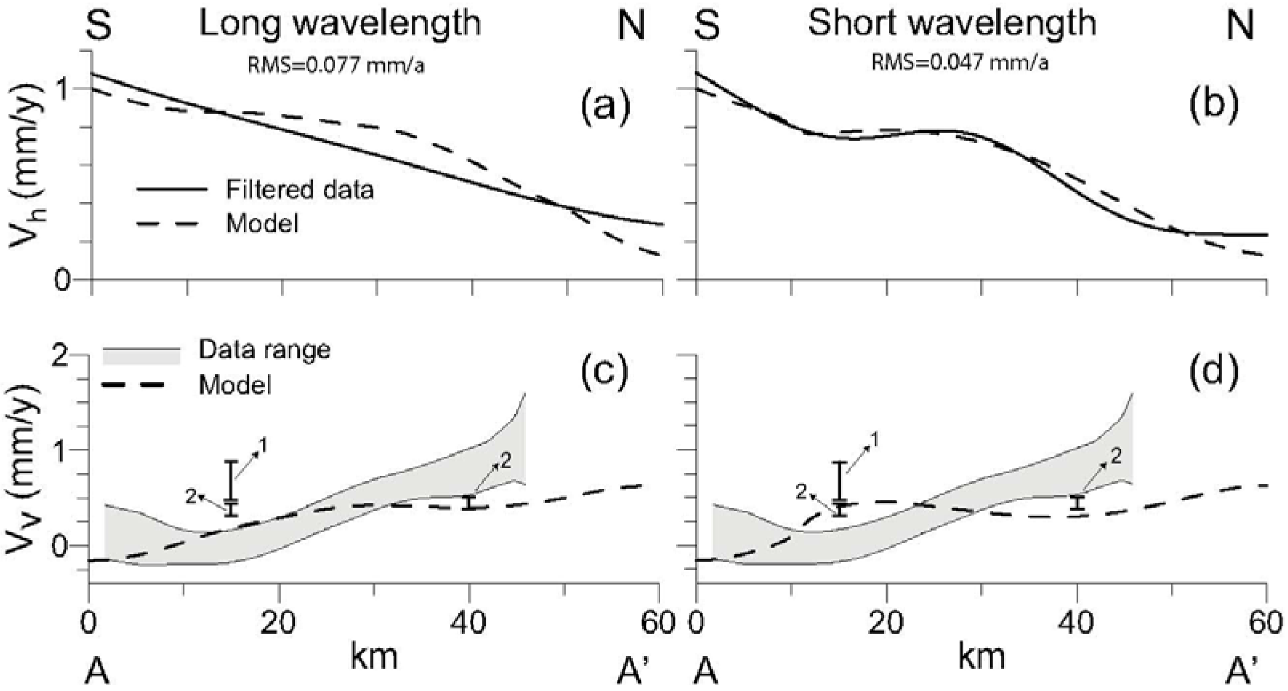

1) Benedetti et al. (2000) 2) Galadini et al. (2005)

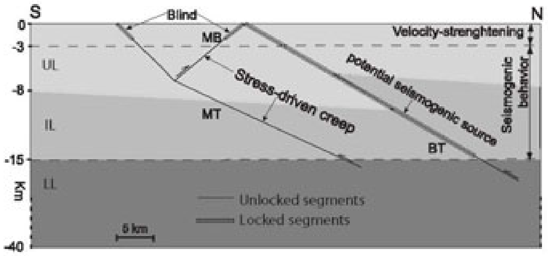
S
N
Blind
MB
MT
BT
Velocity-strenghtening
Seismogenic behavior
potential seismogenic source
Stress-driven creep
UL
IL
LL
0
-3
-8
-15
-40
Km
5 km
Unlocked segments
Locked segments

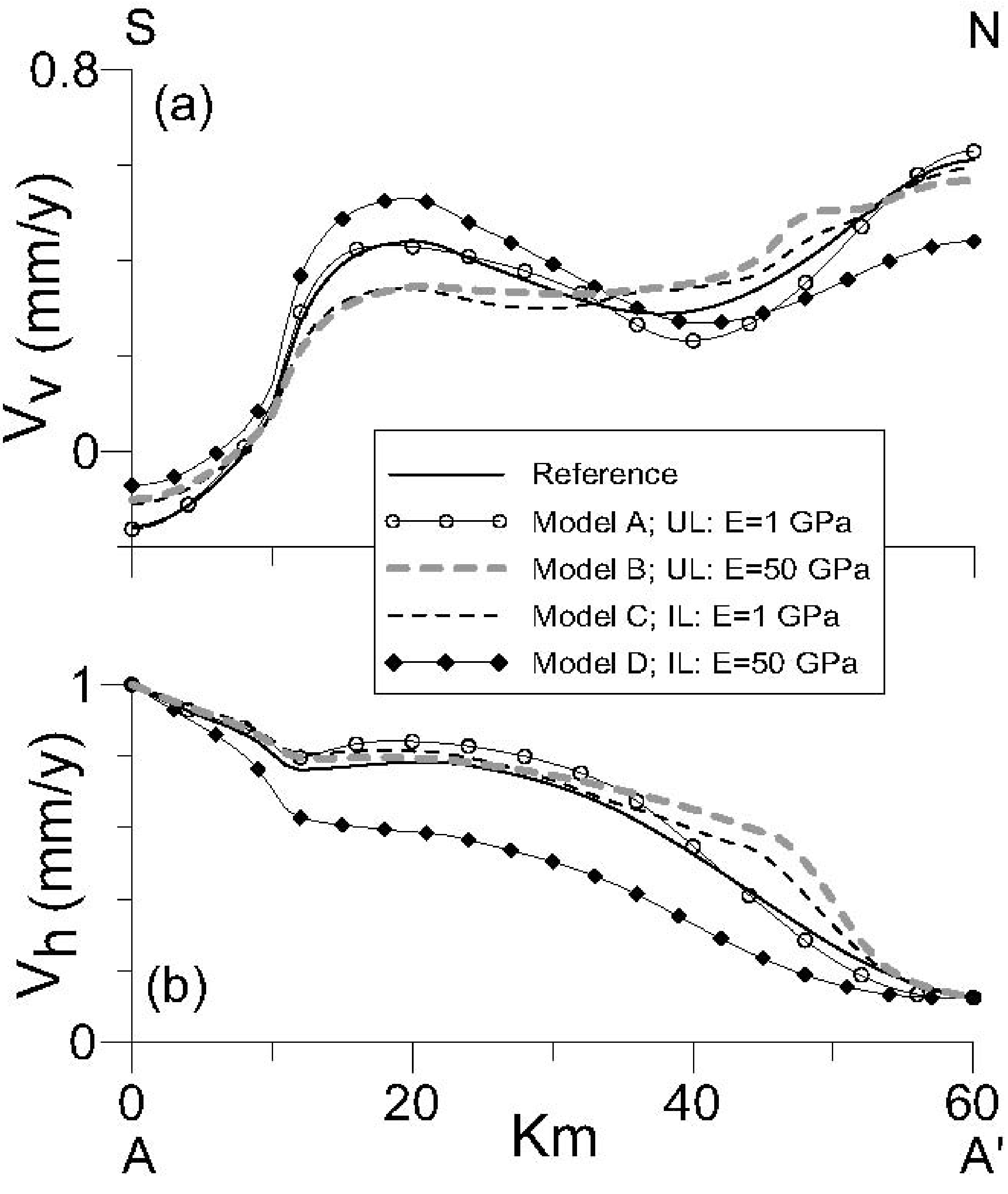
S
N
0.8
(a)
Vv (mm/y)
0
Reference
Model A; UL: E=1 GPa
Model B; UL: E=50 GPa
Model C; IL: E=1 GPa
Model D; IL: E=50 GPa
1
Vh (mm/y)
(b)
0
0
20
40
60
Km
A
A'